

Theoretical Analysis and Experimental Demonstration of a Chirped Pulse-Train Generator and its Potential for Efficient Cooling of Positronium

K. Yamada¹, Y. Tajima², T. Murayoshi¹, X. Fan^{1,†}, A. Ishida¹, T. Namba³, S. Asai¹,
M. Kuwata-Gonokami¹, E. Chae^{1,2,4,5}, K. Shu^{1,2,4} and K. Yoshioka^{2,4,*}


¹Department of Physics, Graduate School of Science, The University of Tokyo, 7-3-1 Hongo, Bunkyo-ku, Tokyo 113-0033, Japan

²Department of Applied Physics, Graduate School of Engineering, The University of Tokyo, 7-3-1 Hongo, Bunkyo-ku, Tokyo 113-8656, Japan

³International Center for Elementary Particle Physics (ICEPP), The University of Tokyo, 7-3-1 Hongo, Bunkyo-ku, Tokyo 113-0033, Japan

⁴Photon Science Center, Graduate School of Engineering, The University of Tokyo, 2-11-16 Yayoi, Bunkyo-ku, Tokyo 113-8656, Japan

⁵Department of Physics, Korea University, Anam-ro 145, Seongbuk-gu, Seoul 02841, Republic of Korea

 (Received 24 January 2021; revised 6 May 2021; accepted 14 June 2021; published 6 July 2021)

We propose an injection-locked pulsed laser with an electro-optic phase modulator in a Ti:sapphire laser cavity to realize both broadband optical spectra and long pulse durations. Further, we experimentally and theoretically demonstrate that the output microsecond-long pulse consists of a train of short pulses in the time domain and a comblike broadband spectrum with fast chirping in the positive and negative directions in the frequency domain. Finally, we discuss the potential of the proposed system for efficient Doppler cooling of positronium, a short-lived exotic atom.

DOI: [10.1103/PhysRevApplied.16.014009](https://doi.org/10.1103/PhysRevApplied.16.014009)

I. INTRODUCTION

Positronium (Ps), the bound state of an electron and a positron, has considerable potential as a probe for fundamental physics. Preparing a cold gas of Ps at temperatures below 10 K is essential for probing fundamental physics. In particular, it improves the precision of $1S$ - $2S$ spectroscopy [1,2], leading to precise testing of the bound-state quantum electrodynamics, owing to the purely leptonic nature of Ps [3,4]. A cold Ps gas is also an essential prerequisite for realizing Bose-Einstein condensation (BEC). Ps is one of the best candidates for demonstrating the first BEC in a system containing antimatter because a high critical temperature is expected (14 K at 10^{18} cm⁻³) and Ps is the easiest antimatter system to produce. A Bose-Einstein condensate of Ps, a coherent matter wave containing antimatter, may be employed to measure the gravitational effect on antimatter using a Mach-Zehnder interferometer [5]. Another unique application of Ps BEC is a “ γ -ray laser” [6–8], used to generate coherent light at 511 keV.

Among the various Ps cooling methods that have been proposed [9–11], laser cooling of Ps using the $1S$ - $2P$ transition has been suggested [12–15] to be the most rapid

method. It is well known that the temperature of a gas of atoms can easily be reduced to the submillikelvin level via laser cooling using a continuous-wave laser [16]. However, the application of laser cooling to Ps, which has not been demonstrated previously, involves the following problems. (1) Inducing the $1S$ - $2P$ resonance of Ps requires deep ultraviolet light at 243 nm. (2) Owing to the nature of a particle-antiparticle pair, Ps is annihilated into γ rays within a lifetime of 142 ns [17]. Therefore, the cooling laser for Ps must have a long pulse duration that is comparable to its lifetime. (3) The Doppler broadening of Ps is large because of its small mass (twice the mass of an electron); hence, an unconventional broadband laser is required. If these problems can be overcome and a rapid frequency chirp can be added for further efficient cooling, it has been numerically shown that a gas of Ps can be cooled down to 10 K [12].

In this study, we propose and demonstrate a pulsed-laser system that satisfies the above-mentioned prerequisites from both theoretical and experimental points of view. To realize a chirped pulse laser with a broadband spectrum, we use the well-known electro-optic sideband generation in a time-resolved manner. The placement of an electro-optic modulator (EOM) in a relatively low-loss laser cavity enhances the sideband generation and leads to a frequency comb with high-order sideband components. Such an optical system is commonly referred to as a frequency

*yoshioka@fs.t.u-tokyo.ac.jp

†Present address: Department of Physics, Harvard University, Cambridge, Massachusetts 02138, USA.

comb generator (FCG) [18]. Here, we apply this technique to the laser cavity of an injection-locked submicrosecond Ti:sapphire laser operating at 729 nm. The laser oscillation dynamics when the EOM is placed in a steady-state optical cavity have been studied extensively [18,19]. However, its behavior in more dynamical cases, for example, when pulsed pumping is applied as in the present study, has not been investigated previously. Here, we numerically formulate its oscillation dynamics in the time and frequency domains. The injection-locked pulsed laser emits submicrosecond-long pulses that consist of a train of short pulses, and the latter exhibits a rapid frequency chirp (several 10–100 GHz/ μ s). Owing to these characteristics, we refer to this unique laser as a chirped pulse train generator (CPTG). We amplify the pulsed laser out from the CPTG using a multipass amplifier followed by nonlinear frequency conversion to generate deep ultraviolet pulses at 243 nm for the future application of laser cooling. The CPTG is a general concept that provides a way to form frequency chirps, and we also discuss the extension and application of this idea to systems beyond positronium cooling.

The paper is organized as follows. In Sec. II, the experimental setup for the CPTG is introduced, followed by amplification and third-harmonic generation. Section III elucidates the underlying theory and the associated numerical simulation of the laser, using the terms and experimental parameters introduced in Sec. II. Section IV presents the experimental results on the characteristics of the prototypical cooling laser in both time and frequency domains, in comparison with those of the numerical simulation. In Sec. V, we discuss the interaction mechanism of the prototypical pulsed laser with Doppler-broadened Ps atoms, having a finite lifetime, for future cooling experiments. Additionally, we discuss how the proposed laser can be improved to realize efficient cooling of Ps atoms from 300 to 10 K. Finally, we summarize the results in Sec. VI.

II. EXPERIMENTAL SETUP

Figure 1 shows an overview of the prototypical cooling laser for Ps. We use a homemade, tunable external-cavity diode laser (ECDL) with a wavelength of around 729 nm (3 times the $1S$ - $2P$ transition wavelength). The ECDL is operated in the free-running mode. Its frequency drift is smaller than 1 GHz over 1 day, which is negligibly small compared with the broadband output of the entire system. A homemade pulsed Ti:sapphire laser is injection seeded through an output coupler by the ECDL. We use a frequency-doubled Nd:YAG pulsed laser with a pulse energy of 15 mJ, pulse duration of 5 ns, and repetition rate of 10 Hz [Minilite(ii), Continuum, Inc.] as a pump laser. Two piezoelectric transducers (PZTs) control the length of the laser cavity using the Hänsch-Couillaud (HC) technique [20] to maintain the injection seeding. A Brewster-cut Ti:sapphire

crystal is employed as a polarizing element to obtain an error signal, which is fed back to the PZTs through a proportional-integral (PI) servo controller followed by a PZT driver. A polarizing beam splitter (PBS) transmitted the P -polarized output pulse to reduce the noise in the error signal caused by the pulsed output. The HC technique worked because of an imperfect polarization extinction ratio of the PBS.

An output coupler with a relatively high reflectivity (98%) is employed to realize a long photon lifetime of the optical cavity. The pulse duration of the output pulse is over 500 ns, which is of the same order as the annihilation lifetime of Ps. In addition, the long photon lifetime of the optical cavity enhances the sideband generation process by an electro-optic modulator. The EOM placed inside the optical cavity broadens the laser spectrum by generating a cascade of sidebands. We use a resonant EOM (quality factor, approximately 65, manufactured by Qubig GmbH), whose resonant frequency is manually tunable. We tune the modulation frequency of the EOM (monitored by a frequency counter) to the free spectrum range (FSR) of the optical cavity (78.7 MHz), which is designed to be comparable to the natural linewidth of $1S$ - $2P$ transition (50 MHz) so that a substantial portion of Ps atoms in the velocity distribution can be cooled: when the FSR is set much larger than the natural linewidth, Ps atoms can resolve the comb structures in a well-separated manner. In this case, no cooling occurs for a fraction of Ps atoms with the Doppler-shifted $1S$ - $2P$ transition frequencies are off resonant with the teeth of the comblike structure, because the laser pulse-induced excitation events interfere destructively. Conversely, an excessively small FSR results in a sparse pulse train in the time domain, as compared to the lifetime of the $1S$ ortho Ps, resulting in a poor cooling rate. This aspect is described in detail in Sec. V.

A high-isolation switch limited the duration of the driving rf power of the EOM to 20 μ s per pulse. The operation of the EOM is initiated 10 μ s before the excitation of the Ti:sapphire crystal in the cavity by controlling the timing of the rf switch relative to that of the Q switch of the pumping laser. The waiting time of 10 μ s, before the excitation, is sufficiently longer than the photon lifetime of the cavity, which is required to establish the maximum sideband order for the injected cw laser. Further, the feedback system, controlling the cavity length, is immune to the pulsed sideband generation owing to the short turn-on time (20 μ s) of the EOM. This pulsed modulation technique has another advantage in terms of reducing the thermal load on the EO crystal and achieving a large modulation depth.

The maximum output energy of the CPTG described above is 500 μ J per pulse at 729 nm, which is limited by the damage threshold of the mirrors constituting the high-finesse ($\mathcal{F} \sim 100$) cavity. We construct a multipass Ti:sapphire amplifier [21] to achieve sufficient

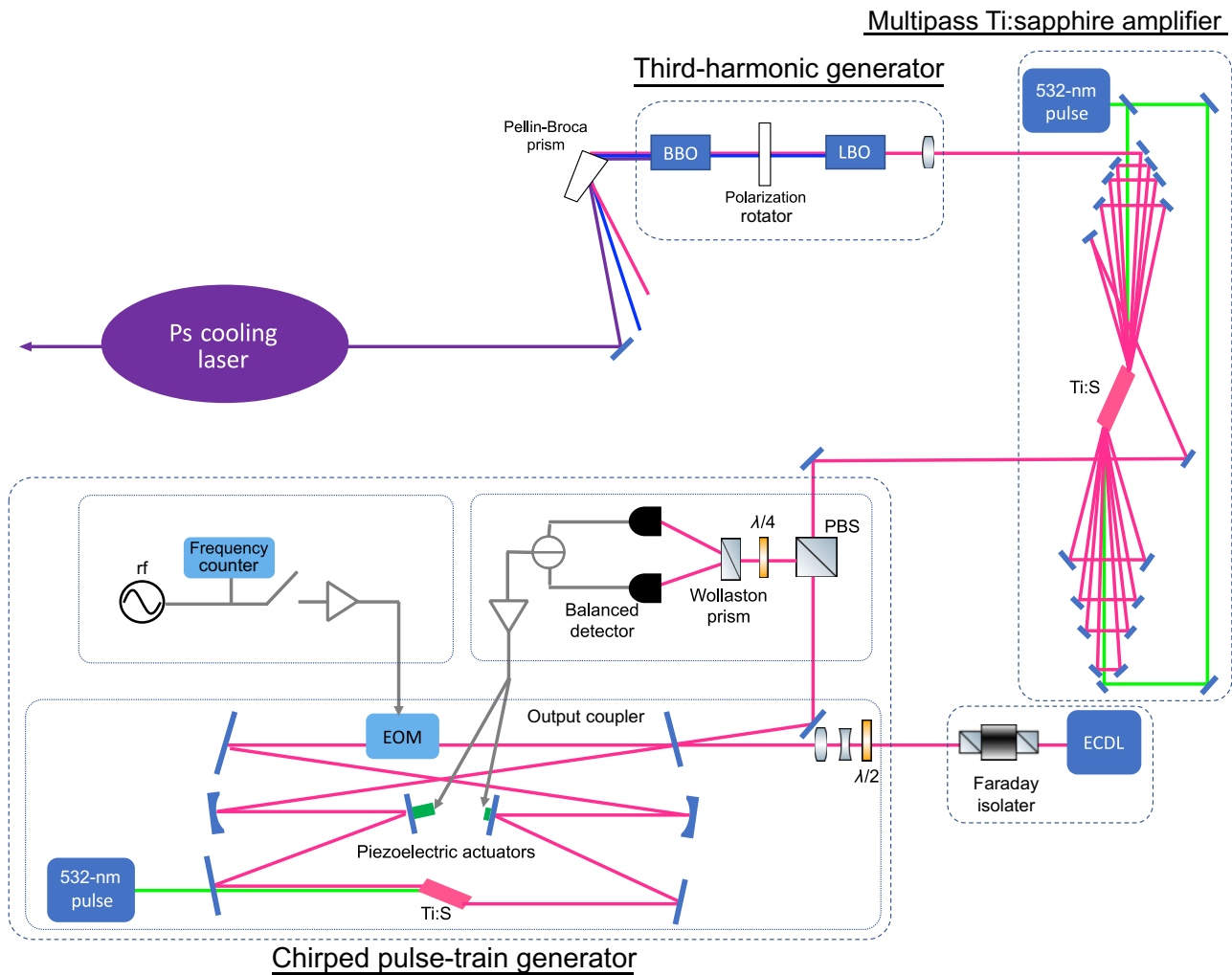


FIG. 1. Schematic of the prototypical cooling laser system. ECDL, external-cavity diode laser; $\lambda/2$, half-wave plate; $\lambda/4$, quarter-wave plate; EOM, electro-optic phase modulator; rf, driving radio frequency; Ti:S, Ti:sapphire crystal; PBS, polarizing beam splitter; LBO, lithium triborate crystal; BBO, β -barium borate crystal.

optical power for the subsequent generation of the third harmonics at 243 nm. A Ti:sapphire crystal is pumped by a frequency-doubled Nd:YAG pulsed laser (Powerlite 7300, Continuum, Inc.) with a maximum pulse energy of 280 mJ. The two pumping lasers are externally triggered by a digital delay generator (DG645, Stanford Research Systems) with a timing jitter of less than 100 ps. After eight rounds of amplification, the pulse energy at 729 nm exceeds 15 mJ.

The amplified pulses are loosely focused by a plano-convex lens ($f = 1000$ mm), and the third harmonics of the amplified pulse are produced by the second-harmonic generation using a type-I LBO crystal, followed by the sum-frequency generation using a type-I BBO crystal. The lengths of the nonlinear crystals are 10 mm for LBO and 2 mm for BBO. For polarization matching of the BBO crystal, we use a crystalline quartz plate that appropriately rotates the polarization of fundamental light and its second

harmonics. A typical pulse energy of the third harmonics is around $600 \mu\text{J}$ (maximum, 1 mJ; intentionally reduced to $600 \mu\text{J}$ to avoid possible optical damage), which is measured after a UV-fused silica Pellin-Broca prism used as a harmonic separator.

To characterize the pulsed laser in the time domain, we use an oscilloscope (bandwidth, 200 MHz) and a photodetector (bandwidth, 2 GHz) to record the waveform of the output pulses at 729 nm. We use another photodetector (bandwidth, 350 MHz) to observe the third-harmonic pulses at 243 nm. In addition, we construct an etalon-based spectrometer [22] to measure the spectrum of the third harmonics at 243 nm on a shot-to-shot basis. We use a Fabry-Perot etalon (Sigmakoki, Co., Ltd.) with a free spectrum range of 500 GHz and spectral resolution of 3.7 GHz (FWHM) at 243 nm. Further details about the measurements are presented in Appendix.

III. THEORETICAL ANALYSIS

This section describes the theory and numerical simulation of the CPTG and its third harmonics after amplification. We perform time-domain analyses to calculate the electric field of these light pulses. The optical spectrum can be evaluated using the Fourier transform of the waveform of the electric field. First, we calculate the electric field in our injected laser cavity without applying the pump laser. This is equivalent to reproducing the FCG, while paying special attention to its temporal characteristics. Second, we calculate the output electric field of the CPTG by applying a pulsed excitation of the gain medium. Third, we calculate the electric field of the third harmonics of the amplified output of the CPTG. In our calculation, the time step is selected to be sufficiently short (approximately 0.8 ps, corresponding bandwidth of 600 GHz) to cover the broad spectrum of this system.

A. Injection of a single-mode cw laser and EO modulation

Initially, we evaluate the dynamics of the electric field in a laser cavity with an EOM. The cavity is injected with a single-mode cw laser beam. Here, we assume that the driving frequency of the EOM is the same as the FSR of the laser cavity. This setup is equivalent to the FCG.

We start the calculation by assuming a ring optical cavity with the injection of a single-mode cw laser, given by Eq. (1):

$$E_{\text{cw}}(t) = E_0 e^{i\omega_0 t} \quad (-\infty < t < \infty). \quad (1)$$

Here, E_0 is the field amplitude and ω_0 is the angular frequency of the input laser.

The electric field inside the laser cavity $E(t)$, before the EOM is turned on, is given by [23]

$$E(t) = \frac{t_r}{\sqrt{(1-r)^2 + 4r \sin^2(\phi/2)}} E_{\text{cw}}(t) \quad (t < 0), \quad (2)$$

where r is the round-trip amplitude reflectance, t_r is the amplitude transmittance of the coupler mirror (see Fig. 1), and ϕ is the phase mismatch between the seed laser and the corresponding longitudinal mode of the laser cavity. $E(t)$ is evaluated at the output coupler mirror. Then, we start to apply continuous phase modulation using the EOM from $t = 0$. The cavity output field is given by Eq. (3). The equation includes the cyclic boundary condition of the optical cavity, optical loss in the optical cavity:

$$E(t) = t_r E_{\text{cw}}(t) + r E(t - T) \times e^{i\beta \sin \Omega t} \quad (0 \leq t). \quad (3)$$

Here, T is the round-trip time, r is the round-trip amplitude reflectivity of the optical cavity, β is the modulation

TABLE I. Parameters used in the numerical simulation.

Round-trip cavity length: L	3.8 m
Transmittance of output coupler: $T_r = t_r^2$	0.02
Round-trip power reflectance: $R = r^2$	0.95
Round-trip power loss	0.03
Round-trip time: T	12.7 ns ($= L/c$)
Free spectrum range (FSR)	78.7 MHz
Modulation frequency: f_m	78.7 MHz
Modulation depth: β	2.3 rad
Photon lifetime of the optical cavity	247 ns
Upper-state lifetime in Ti:sapphire: τ	3.2 μ s
Saturation fluence: J_s	1.4 J/cm ² at 729 nm

depth of the EOM, $\Omega (= 2\pi f_m)$ is the angular modulation frequency, and f_m is the modulation frequency. The parameters for the present simulation are listed in Table I.

By substituting Eqs. (1) and (2) into Eq. (3) recursively and expanding the equation explicitly, we can verify that all the terms of Eq. (3) have a common phase term oscillating at the optical frequency of the input single-mode cw laser ($= e^{i\omega_0 t}$). Therefore, we can safely exclude the phase term in the following. This corresponds to calculating the response function of the FCG with respect to the optical frequency of the single-mode seeding laser. The output field can be obtained by evaluating $t_r E(t)$.

In general, the optical elements in the laser cavity cause the group velocity dispersion, leading to a frequency mismatch between the longitudinal modes of the cavity and the higher-order sidebands. In the present case, the mismatch is found to be negligible, and therefore the effect of the group-velocity dispersion in the cavity is ignored in the calculations. When it is necessary to deal with a much wider bandwidth than in the present case, we need to compensate for the dispersion.

Using the equations above, we investigate the properties of the FCG in the time domain. We focus on the results of the simulation under the following ideal conditions: we ignore the phase noise of the seed laser, and we assume that the frequency of the laser and the modulation frequency match perfectly with the longitudinal modes of the optical cavity. When the system reaches a steady state in a few microseconds, $E(t)$ becomes

$$E(t) = \frac{t_r}{1 - r e^{i\beta \sin \Omega t}} E_{\text{cw}}(t). \quad (4)$$

Figure 2 shows the simulated output in the time domain. The output consists of a train of short pulses at even intervals. The time interval of the short pulses is $T/2 \sim 6.4$ ns. This means that a pair of short pulses is present inside the optical cavity. The waveform of each of the short pulses is given by the following equation [24]:

$$P(t) \propto [t^2 + 1/(2\beta f_m \mathcal{F})^2]^{-2}, \quad (5)$$

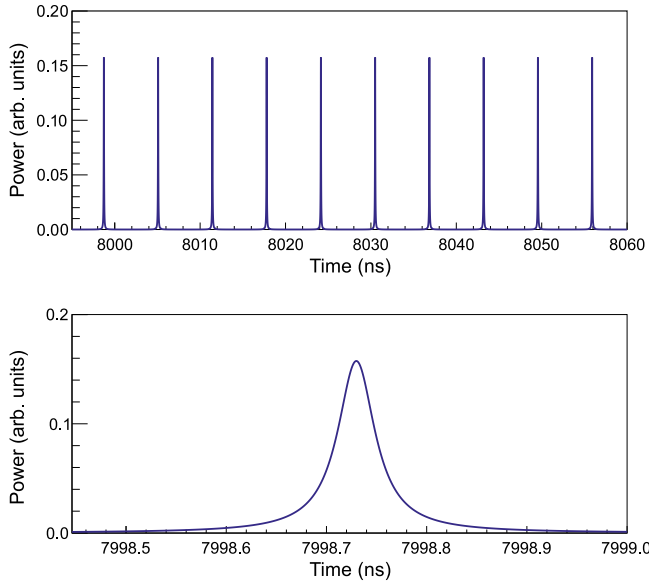


FIG. 2. Output of the FCG in the time domain. Top panel: trains of short pulses. Bottom panel: magnified view of a representative short pulse, whose waveform is given by Eq. (5).

where \mathcal{F} is the finesse of the optical cavity. In the present case, the calculated pulse duration (FWHM) of the short pulse at 729 nm is 45 ps.

Next, we analyze the output in the frequency domain by applying the Fourier transform to the time-domain result. We set the interval of the rectangular window function of the Fourier transform to be much longer than the round-trip time of the optical cavity. The top panel of Fig. 3 compares the spectra of the FCG before and after the cavity-enhanced EO modulation. The middle panel of Fig. 3 shows the magnified spectrum of the FCG. Owing to the cavity-enhanced phase modulation, the spectrum of the FCG shows a comblike structure, which consists of evenly spaced sidebands up to high orders, as the name suggests. The output power of the k th sideband is $P_k \propto \exp(-2|k|\pi/\beta\mathcal{F})$ [18]. The contour of the spectrum is given by the following function with good approximation:

$$P(\nu - \nu_0) \propto \exp\left(-\frac{2|\nu - \nu_0|\pi}{\beta f_m \mathcal{F}}\right), \quad (6)$$

where ν is the optical frequency and ν_0 is the optical frequency of the input single-mode laser.

Next, we set the time window function as a rectangular window with a duration of $T/2$ (approximately 6.7 ns) to evaluate the spectrum of each short pulse. Performing the Fourier transformation using a window function with a short time interval is an effective way to evaluate the time-varying optical spectrum of this system. The bottom panel of Fig. 3 shows the spectrum of each pulse that constitutes a pulse pair. One is composed of only positive orders

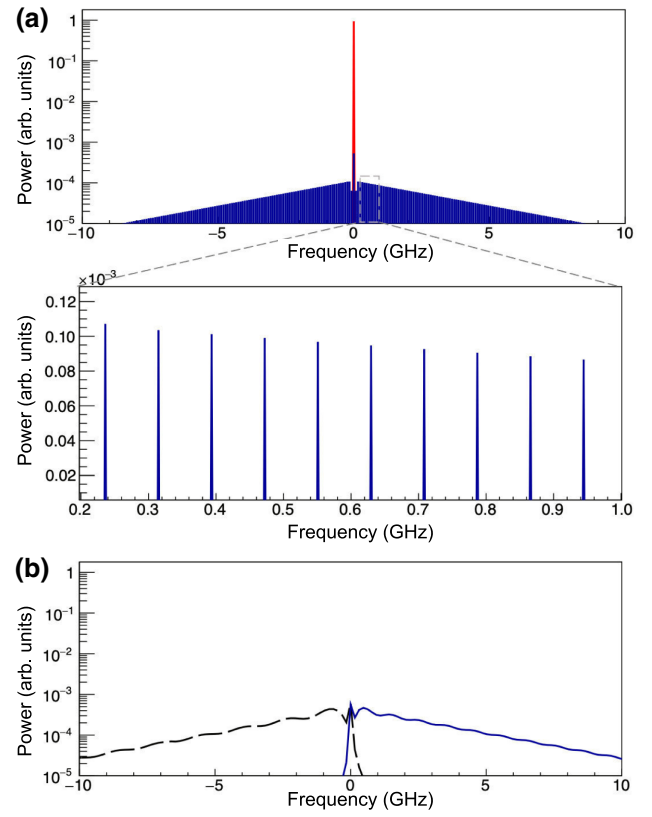


FIG. 3. Output of the FCG in the frequency domain. The zero frequency is set to the optical frequency of the seed laser. (a) Upper panel: entire spectrum before and after EO modulation. The red curve represents the spectrum before the spectral broadening by the EOM, while the blue curve represents the spectrum after the broadening. Lower panel: magnified view of the spectrum, where evenly spaced sidebands can be seen. (b) Spectrum of a typical pulse pair. One is composed only of positive frequency components (solid curve), whereas the other is composed only of negative frequency components (dashed curve).

of sidebands, while the other is composed of only negative ones. Therefore, the FCG outputs short pulses with higher frequencies and lower frequencies alternately [25]. The contour of the FCG spectrum, i.e., the contour of the integrated spectrum of all the short pulses, is given by Eq. (6); however, the spectrum of each short pulse is approximately given by either the positive or the negative half of the contour, as can be seen in Fig. 3(b). Therefore, the bandwidth of a single short pulse is given by the following equation, which represents the half width at half maximum of Eq. (6):

$$\nu_{\text{FWHM}}^{\text{pulse}} = \frac{\beta f_m \mathcal{F} \ln 2}{2\pi} \text{ (Hz)}. \quad (7)$$

In the present calculation, the typical bandwidth is $\nu_{\text{FWHM}}^{\text{pulse}} = 2.4$ GHz at 729 nm.

B. Pulsed operation: CPTG

Next, we pump the Ti:sapphire crystal in the FCG by using a pulsed laser to understand how the CPTG works. The optical amplification by the Ti:sapphire crystal is governed by the following set of equations.

Equation (8) expresses the condition for the amplification timing:

$$J_{\text{sto}}(t) = \begin{cases} 0 & (t < T_0^{\text{gain}}) \\ J_{\text{sto}} & (t = T_0^{\text{gain}}) \end{cases} \quad (8)$$

Here, J_{sto} is the equivalent fluence of the stored energy in the upper level in the Ti:sapphire crystal. Further, T_0^{gain} is the amplification timing by the nanosecond pump laser (second harmonics of the Nd:YAG laser). We assume that the amplification by the Ti:sapphire crystal occurs instantaneously after the excitation. Thus, we ignore the pulse width of the pump laser (approximately 5 ns). Before the amplification, we continue the simulation until the system reaches a steady state, and we then applied a pulsed gain. The typical amplification timing T_0^{gain} is 8 μs , which is 40 times longer than the photon lifetime in the optical cavity and is sufficient to reach a steady state.

Equation (9) expresses the law of conservation of energy in a gain medium and the energy loss by spontaneous emission:

$$J_{\text{sto}}(t + dt) = [J_{\text{sto}}(t) - J_{\text{out}}(t) + J_{\text{in}}(t)] \times e^{-dt/\tau}, \quad (9)$$

where dt is the time step of the simulation and τ is the upper-state lifetime of the Ti:sapphire crystal. $J_{\text{in}}(t)$ is the time-sliced fluence of the input pulse at 729 nm,

$$J_{\text{in}}(t) = \frac{\epsilon_0}{2} |E(t)|^2 c dt, \quad (10)$$

where ϵ_0 is the permittivity of vacuum and c is the speed of light. Equation (11) is the Frantz-Nodvic equation for the sliced-square input pulse [26], where $J_{\text{out}}(t)$ is the time-sliced fluence of the output pulse and J_s is the saturation fluence. Equation (11) assumes that the time width (dt) of the sliced-square input pulse is much shorter than τ .

$$J_{\text{out}}(t) = J_s \log[1 + e^{J_{\text{sto}}(t)/J_s} (e^{J_{\text{in}}(t)/J_s} - 1)]. \quad (11)$$

Equation (12) expresses the amplitude gain for the input laser:

$$G(t) = \sqrt{J_{\text{out}}(t)/J_{\text{in}}(t)}. \quad (12)$$

Equations (9)–(12) hold when $-\infty < t < \infty$.

Now, the output field of the CPTG, $t_r E(t)$, can be calculated using Eq. (13), where the amplitude gain is added to

Eq. (3):

$$E(t) = t_r E_{\text{cw}}(t) + E(t - T) r G(t) \times e^{i\beta \sin \Omega t} \quad (0 \leq t). \quad (13)$$

Figure 4(a) shows the power waveform of the output pulse from the CPTG. The overall shape indicates that the duration of the output contour is approximately 1 μs , which is determined by the photon lifetime of the laser cavity and the gain reduction by the stimulated emission in the gain medium. If we take a closer look, we can see that

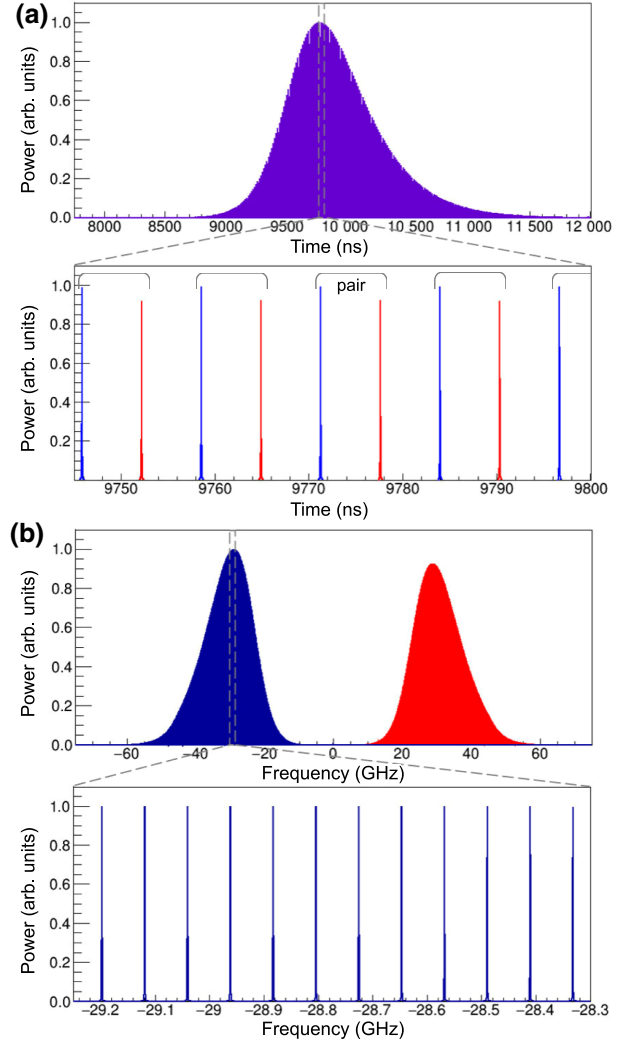


FIG. 4. Calculated output characteristics of CPTG. (a) Power waveform of the output pulse. The time origin is defined as the turn-on time of the EOM. The pulsed optical gain by the pump pulse is applied at 8 μs . The lower figure shows a magnified view of the waveform. Red and blue colors of the pulse pairs indicate higher and lower frequency components shown in (b). The spectra of selected pairs are presented in Fig. 5. (b) Spectrum of the optical pulse shown in (a). The zero frequency is set to the optical frequency of the seed laser. The lower figure shows a magnified view near the peak of the lower frequency component in the upper figure.

the pulse is composed of a train of short pulses at equal intervals. The CPTG outputs short pulses with higher frequencies and lower frequencies alternately in the same way as the FCG [25], which we confirm by taking the Fourier transform of each short pulse.

Figure 4(b) shows the spectrum of the output pulse of the CPTG. The time window function for the Fourier transform is set to cover the long pulse almost entirely. The spectrum has a characteristic contour with two peaks, and evenly spaced sidebands are present inside the contour. Therefore, the CPTG maintains the comblike spectrum even after the pulsed gain is applied. However, the entire structure of the spectrum calculated as Eq. (6) is strongly affected by the pulsed operation. Specifically, the temporal behavior of the short pulses in the long pulse results in the characteristic contour, as discussed in the following.

Figure 5 shows the calculated optical spectrum of typical pairs of consecutive short pulses inside the long contour [red and blue colored pulses in the magnified view in Fig. 4(a)] at different times. The spectrum at 8000 ns is obtained prior to the pulsed gain excitation [see Fig. 3(b)]. Owing to the stimulated emission in the Ti:sapphire crystal, the pulse energy of the short pulses gradually increases. After the pump energy stored in the Ti:sapphire crystal is extracted, the pulse energy of the short pulses gradually decreases with the loss in the optical cavity. It is worthwhile to note that the continuous phase modulation shifts the laser power further from lower sidebands to higher sidebands. Namely, the pulsed gain intensifies the spectral broadening of the FCG. In addition, a rapid frequency chirp appears in the positive and negative directions through a combination of the pulsed gain and the phase modulation. Specifically, the FSR gives the number of times a pulse passes through the EOM per second, and its peak optical frequency is shifted by approximately βf_m in each phase modulation event. Therefore, the chirp rate is given by

$$\text{chirp rate} = \pm \beta f_m \text{FSR (Hz/s)}. \quad (14)$$

In the present case, the typical chirp rate is ± 14 GHz/ μ s at 729 nm. This rapid frequency chirp is a unique feature, found in a laser cavity with both continuous phase modulation and pulsed gain. This unique feature cannot be realized with the FCG [18,25]. The frequency chirp continues to occur as long as the pulsed oscillation lasts. Owing to their

pulsed nature and the rapid chirp, the comblike optical frequencies survive for a limited time only. For this reason, the calculated linewidths of the comb teeth for both 729 and 243 nm are 0.9 MHz. By taking the third harmonics of the amplified CPTG, the chirp rate is tripled and becomes ± 42 GHz/ μ s at 243 nm. The details for simulating the amplification and the third harmonics are described in Sec. III C.

While the overall spectrum of the CPTG has a unique structure, the spectra of short pulses, composing the CPTG, exhibit a structure similar to those without the pulsed gain. The main differences are the amplitude distribution and the absence of the lower orders of sidebands. The latter is induced by the frequency chirp and pulsed gain. The continuous input from the seed laser contributes to the lower orders of sidebands; however, this contribution is negligible. The contour in the higher orders of sidebands is given by the same spectral decay constant as Eq. (6), $\beta f_m \mathcal{F} / \pi$. Therefore, the bandwidth of the short pulse is given by Eq. (7), $\nu_{\text{FWHM}}^{\text{pulse}} = \beta f_m \mathcal{F} \ln 2 / 2\pi = 2.4$ GHz, with a good approximation. If we calculate the third harmonics of the amplified short pulse, then the bandwidth becomes 17 GHz at 243 nm. The corresponding pulse duration (FWHM) at 243 nm is 6.4 ps.

In summary, our numerical simulation of the CPTG showed that this pulsed laser has the following main features: (a) a train of short pulses in a microsecond-long contour, (b) a comblike broadband spectrum with two characteristic peaks, and (c) a rapid frequency chirp in the positive and negative directions.

C. Amplification and third-harmonic generation

The simulation above is conducted for the CPTG and not for a cooling laser for Ps, i.e., the third harmonics of the multipass amplified CPTG. The procedures for simulating the cooling laser are described in the following.

1. We compare the temporal profile of the simulation with the experimentally measured power waveform of the CPTG and determine the free parameter for the simulation. The only free parameter is J_{sto} , which is the equivalent fluence of the stored energy in the upper level in the Ti:sapphire crystal. When we compare the simulated power waveform with the experimental data, we look

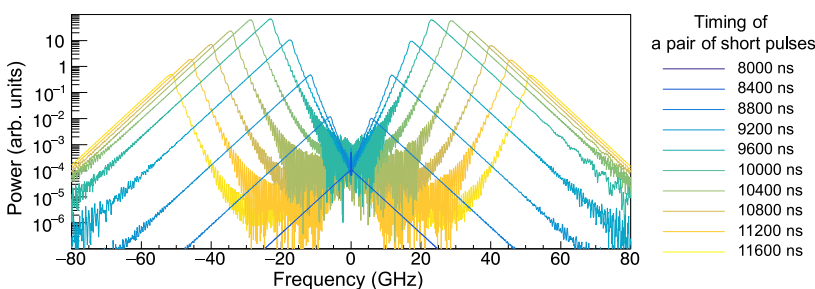


FIG. 5. Simulated spectra of the pairs of short pulses in the long pulse at different timings. The zero frequency is set to the optical frequency of the seed laser. The timing of the pair of short pulses shown in the legend corresponds to the time defined in Fig. 4. A timing of 8000 ns is just before the pulsed gain is applied. The spectral broadening by the cavity-enhanced modulation and a rapid frequency chirp in the positive and negative directions can be seen.

only at the envelope of the long pulse. This is because the measurement bandwidth is sufficiently wide to resolve the contour but not for the short pulses inside the long pulse.

2. To simulate the multipass amplification, we apply a step-function-like window function to the long pulse of the CPTG. We calculate only the spectrum of the amplified part of the long pulse and ignore the nonamplified part.

3. To calculate the third harmonics, we cube the electric field at each temporal point.

4. We apply an appropriate window function to the electric field and perform the Fourier transformation to calculate the corresponding spectrum.

5. We convolve the simulated spectrum with the spectral resolution of the spectrometer.

IV. EXPERIMENTAL RESULTS

We conduct experiments to demonstrate the three above-mentioned properties of the CPTG (see Sec. III B) by measuring the time profile of the CPTG and the temporal and spectral characteristics of the third harmonics of the multipass amplified CPTG. The potential use of the third-harmonic pulses as a prototypical cooling laser for cooling Ps at 243 nm is discussed in Sec. V.

A. Short pulses in the long-pulse contour

We observe the power waveform of the CPTG at 729 nm. The bandwidth of the detector is sufficiently wide for the observation of the width of the contour of the short-pulse train, but not for that of the short pulses inside the contour. Therefore, we can obtain the interval of the short pulses, but we do not resolve their exact shape. Figure 6 shows the power waveform of the CPTG at 729 nm and its magnified view. The oscilloscope is triggered by the turn-on TTL pulse for the Q switch of the pump laser, and the time shown in Fig. 6 is the time elapsed since the trigger. We observe a long pulse with deep amplitude modulation. The duration of the contour is around 1 μ s, which is determined by the photon lifetime of the laser cavity and the gain reduction due to the stimulated emission in the gain medium. The lower panel of Fig. 6 shows a magnified view of the long pulse around 2500 ns. We can see equally spaced short pulses inside the contour. The interval of the short pulses is 6 ns, which is a half of the round-trip time of the cavity. This interval is consistent with the numerical simulation. Thus, we confirm the characteristics of the CPTG in the time domain, i.e., a train of short pulses inside a microsecond-long contour.

B. Broadband spectrum

We observe the spectrum of the third harmonics of the amplified CPTG using an etalon-based spectrometer. The details of the spectrometer and its calibration procedure are presented in Appendix.

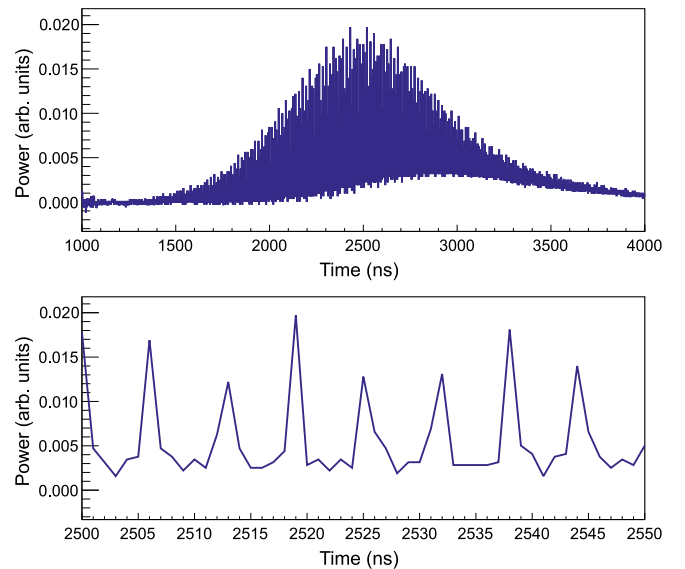


FIG. 6. Power waveform of the CPTG at 729 nm. Top panel: entire pulse. Bottom panel: magnified view around 2500 ns. Due to technical and experimental limitations, the Q -switch timing of the pump laser is adopted as the time origin, and thus the time presented here differs from that of the numerical simulation.

Figure 7 shows the spectrum of the entire pulse at 243 nm with different modulation frequencies around the FSR of the optical cavity. Two characteristic peaks are observed, as shown in our simulation (Fig. 4). The peak structure in the spectrum remains after the third-harmonic generation process because the positive and negative frequency components of the CPTG do not overlap in the time domain. As we have a low-frequency resolution of around 20 GHz compared to the 78-MHz interval of the sidebands,

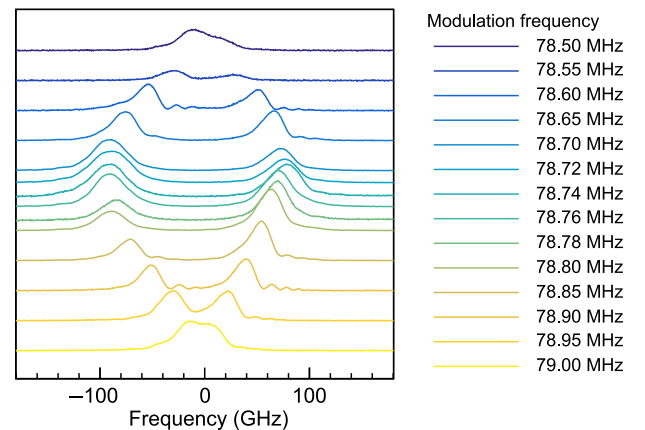


FIG. 7. Spectrum of the entire pulse of the third harmonics of the amplified CPTG with different modulation frequencies. The zero frequency is set to the peak position of the spectrum taken without the EO modulation.

we cannot resolve the comblike structure of the spectrum. The highest orders of the sidebands are achieved when the EOM is driven at 78.74 MHz, which is consistent with an independent measurement of the FSR of the optical cavity [78.7(1) MHz]. Subsequently, we fix the EO modulation frequency at 78.74 MHz.

The maximum order is inversely proportional to the mismatch between the driving frequency and the FSR of the laser cavity. In addition, it is possible to generate either only positive or only negative sidebands by adjusting the relative frequency between the cw laser and the longitudinal mode of the cavity, as well as between the rf modulation frequency and the FSR.

We compare the spectrum of the third harmonics with our numerical simulation, as shown in Fig. 8. The maxima of all the three spectra are normalized to unity. The blue curve represents the instrumental function of the spectrometer to be convolved to the numerical simulation. The black curve represents the numerically simulated spectrum of the third harmonics of the CPTG convolved with the instrumental function of the spectrometer. This spectrum is generated as discussed in Sec. III C. The red curve represents the experimentally measured spectrum. The experimental results and numerical simulation show reasonable agreement. Our calculation shows that the positive-negative asymmetry of the structure of the spectrum depends on the timing of the nanosecond pump laser of the CPTG. According to our numerical simulation described above, two short pulses are present 6 ns apart inside the CPTG. One is composed of positive orders of sidebands generated by the EOM, while the other is composed of negative orders of sidebands. If the positive short pulse is amplified first by the pumped crystal, the positive half of the output spectrum has higher power, and if the negative short pulse is amplified first, the negative half of the output spectrum has higher power. Therefore, the timing of the pump laser of the CPTG in the numerical simulation is tuned (in the range of 6 ns) to reproduce the experimental result.

C. Fast chirp

Next, we experimentally demonstrate the rapid frequency chirp of the CPTG. In this study, we measure the rapid frequency chirp inside the microsecond-long contour, indirectly, by changing the timing of the pump laser for the multipass Ti:sapphire amplifier with respect to the timing of the pump laser for the CPTG. The partially amplified pulsed laser of the CPTG is sent to the THG system, and we measure the spectrum of the third harmonics at 243 nm using the etalon-based spectrometer. The rise time of the amplification is around 20 ns, which is given by the convolution of the pulse width of the pump laser (5 ns) and the traveling time of the path length of the amplification system (20 ns). The fall time of the amplification is determined by the pulse duration of the input, and the gain reduction that is deduced from the amplification process. Thus, the delayed multipass amplifier acts as an optical shutter to find the spectral dynamics in the microsecond-long contour. The spectrum of the partially amplified laser pulse is the integration of all the spectra of the short pulses after the amplification timing. By changing the timing of the amplifier and measuring the spectrum of the partially amplified pulse, we time-resolve the optical spectrum.

Figure 9 shows the result. The top panel shows the time profile of the third-harmonic pulse. We change the timing of the pump laser for the multipass amplification with respect to the timing of the pump laser of the CPTG from 1.1 to 1.85 μs with an interval of 50 ns. The bottom panel shows the time dependence of the spectrum of the pulse at 243 nm, where we can find the rapid chirp effect in the positive and negative frequency directions inside the long pulse. The red curves represent the simulated peak frequencies of the partially amplified pulse at a chirp rate of ± 42 GHz/ μs at 243 nm. The experimental result shows reasonable agreement with the numerical simulation. The agreement also implies that the frequencies of the ECDL and the EO modulation frequency are tuned to the FSR of the optical cavity with sufficient precision and stability.

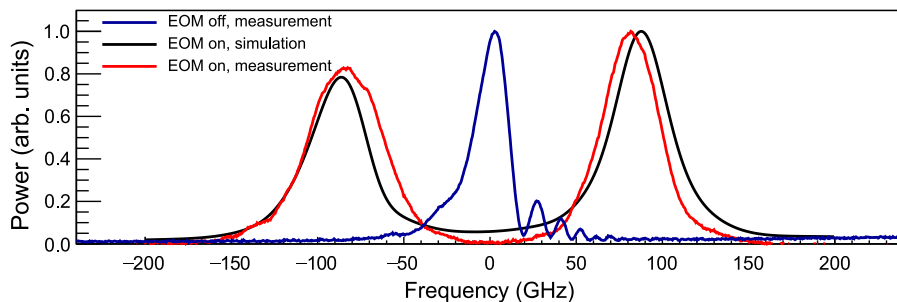


FIG. 8. Comparison of the measured spectrum of the third harmonics of the amplified CPTG with our simulation. The modulation frequency of the EOM is 78.74 MHz. The blue curve represents the instrumental function of the spectrometer for 243 nm. The peak position is set as the origin of the horizontal axis. The black curve represents the numerically simulated spectrum of the third harmonics of the CPTG convolved with the instrumental function of the spectrometer. The red curve represents the experimentally measured spectrum of the third harmonics of the amplified CPTG.

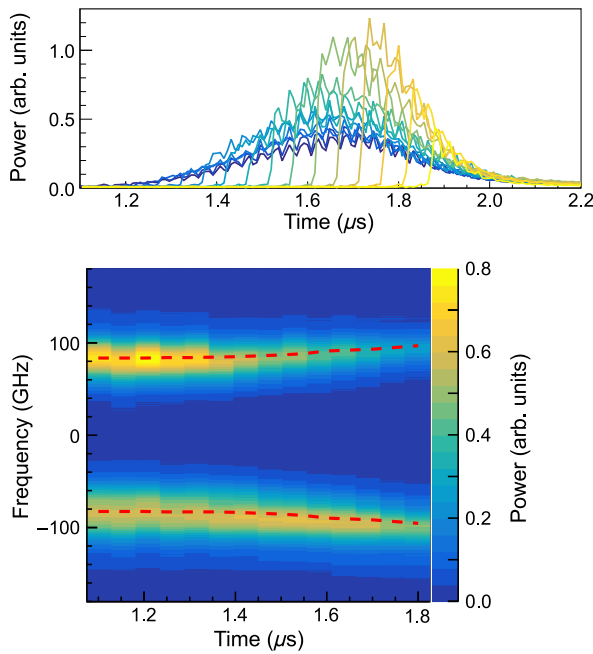


FIG. 9. Demonstration of the rapid frequency chirp of the third harmonic laser pulse at 243 nm. Top panel: power waveform. The waveforms with different colors designate pulses with different timings for multipass amplification. The waveforms are averaged over 100 shots. Bottom panel: time dependence of the spectrum of the partially amplified pulse. The red dashed curves represent the simulated peak frequencies of the partially amplified pulse.

V. DISCUSSION

In this section, we discuss the application of the CPTG to laser cooling of Ps. First, we evaluate the performance of the third harmonics of the amplified CPTG as a prototypical cooling laser for Ps. Next, we present a roadmap for further improving the present CPTG to realize a more efficient laser cooling of Ps.

We demonstrate the following three characteristics of the prototypical cooling laser at 243 nm: (a) a train of short pulses inside the 500-ns-long contour (FWHM); the duration of the contour is approximately 3 times as long as the annihilation lifetime of Ps. This is sufficiently long to cool Ps from 300 to 10 K, if a sufficiently broadband spectrum and a rapid frequency chirp are available such that the laser can sweep the whole Doppler-broadened spectrum of the $1S$ - $2P$ transition. (b) Spectral broadening by EO modulation spanning over 200 GHz in total and two characteristic peaks in the spectrum. For comparison, the Doppler width (FWHM) of the Ps at 300 K is 460 GHz. According to our simulation, the instantaneous spectral width (FWHM) is 17 GHz for each pulse (see Sec. III B). The wide spectral coverage is realized by the frequency chirp. (c) A rapid frequency chirp (± 42 GHz/ μ s) in the positive and negative directions. A frequency chirp over the whole range of

the Doppler profile within the annihilation lifetime maximizes the cooling efficiency. All three characteristics are essential for efficient laser cooling of Ps.

Additionally, it is necessary to assess how densely the cooling laser fills the frequency space because it cannot tune the laser frequencies continuously. The frequency chirp occurs while maintaining the comblike structure defined by the CPTG. Therefore, no optical power is available between the comb teeth of the cooling laser. In the time domain, a train of short pulse pairs arrives at the Ps atoms repeatedly every $1/\text{FSR}$ s. The coherent addition of these pulses results in the comb structure in the frequency domain. In the present case, the calculated linewidth of a comb tooth is 0.9 MHz with respect to a FSR of 78.7 MHz, as discussed before. With such a sparse frequency distribution, the cooling laser may seem to interact with only selected Ps atoms, whose Doppler-shifted transition frequencies coincide with one of the comb teeth. However, the natural linewidth of the cooling transition (50 MHz for the $1S$ - $2P$ transition) compensates the sparsity. If the FSR is comparable or smaller than the natural linewidth, then nearly all the Ps atoms lying within the spectral region of the cooling laser can interact with the laser pulses. Excessively small FSRs result in insufficient cooling efficiency because of the finite lifetime of the $1S$ state (142 ns), which is a unique characteristic inherent to exotic atoms. Therefore, the FSR should be much larger than typically the inverse of the lifetime (7 MHz). For these reasons, FSRs of several tens of MHz are suitable for using the CPTG in the laser cooling of Ps atoms.

We can evaluate the effects described before by convolving the spectrum of the incoming laser with the natural linewidth of the $1S$ - $2P$ transition. The resulting spectrum effectively shows the probability distribution of Ps atoms that can interact with the cooling laser. Figure 10(a) shows an expanded view of the current prototypical cooling laser's calculated spectrum and the normalized absorption probability distribution of the Ps atoms. The filled distribution indicates that the proposed laser fully interacts with the Doppler-broadened Ps atoms within its spectral range. Figure 10(b) compares the group of Ps atoms that interact with the prototypical cooling laser and the Doppler profile of Ps at 300 and 10 K. The central frequency of the cooling laser is red detuned by 200 GHz from the Doppler-free $1S$ - $2P$ transition frequency of Ps to perform chirp cooling, which is primarily done with the positive chirped components. By evaluating the ratio between the spectral widths, we estimate that the laser can cool approximately 5.4% of the total population at 300 K. Comparing the signal-to-noise ratios in typical Doppler spectroscopy experiments [22,27], we find that this amount of change induced by the cooling laser is detectable. This evaluation is optimistic and not complete. Further experimental investigations and Monte Carlo simulations will be necessary to assess the feasibility of performing practical

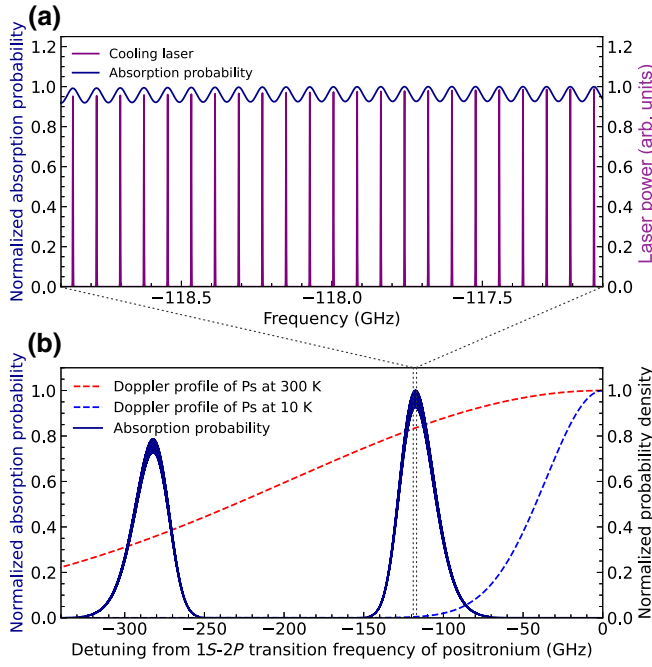


FIG. 10. (a) Normalized absorption probability distribution of the Ps atoms for prototypical laser cooling. The purple curves show a part of the calculated optical spectrum of the cooling laser. The blue curve represents the corresponding probability distribution of the Doppler-shifted Ps atoms, normalized to unity. (b) Expanded view of the normalized probability distribution for absorption (solid curve), compared with the Doppler profiles at 300 K (red dashed curve) and 10 K (blue dashed curve). The Doppler-free $1S-2P$ transition frequency is denoted as the origin of the horizontal axis.

experiments. Demonstration of laser cooling of Ps atoms, using the current prototypical laser, will be an essential step forward.

For more efficient cooling of the entire Ps gas, it is essential to configure a laser with a broader spectrum and a more rapid frequency chirp at 243 nm. Here, we discuss

the guidelines for improving the present CPTG to realize a more efficient laser cooling of Ps. Based on the results of this study, we can design an optical system with the desired temporal and spectral structures. The duration of the pulsed laser is typically given by the photon lifetime of the laser cavity and the gain reduction due to the stimulated emission in Ti:sapphire. The bandwidth and chirp rate of the CPTG are given by Eqs. (7) and (14), respectively, as discussed in Sec. III.

A broader spectrum and a more rapid frequency chirp can be achieved as follows. The bandwidth of the pulsed-laser spectrum is linearly proportional to the modulation depth β , modulation frequency f_m , and finesse \mathcal{F} . Therefore, a broad spectrum can be obtained by increasing these parameters. A greater modulation depth typically leads to thermal instability of the EOM; however, applying EO modulation only for a short yet sufficient duration (in this study, $10 \mu\text{s}$ in a repetition period of 100 ms, i.e., with a duty ratio of 10^{-4}) allows large and stable modulation. We place an EOM inside the ring cavity in this study; however, if the EOM is placed inside a linear cavity with the same cavity length, the total amount of phase modulation per unit time can be doubled. With a higher modulation frequency f_m , a broad spectrum can be obtained albeit with a sparser interval between the comblike lines. In this case, the interval can be reduced by placing another EOM with a smaller modulation frequency outside the laser cavity [28]. In addition, it is possible to obtain a larger effective finesse by employing a CW amplifier inside the laser cavity [19]. Special care must be taken to compensate the group-velocity dispersion in the laser cavity to realize a sufficiently large bandwidth of hundreds of gigahertz.

The requirements for the cooling laser of Ps are proposed in Ref. [12]. Table II summarizes the estimated future specifications of the present CPTG in comparison with the requirements for Ps BEC. We expect that the laser requirements for Ps BEC can be achieved by

TABLE II. Present and estimated future specifications of the cooling laser for Ps and requirements for Ps BEC [12]. As the pulse energy, half of the total pulse energy is listed for present and future specifications. This is because we mainly use the positively chirped frequency components of the CPTG in the chirp cooling of Ps. Both the time duration and the spectral width are shown in terms of the FWHM. The change in the Doppler shift induced by the laser cooling (300 to 10 K in 300 ns) corresponds to a frequency shift of $+755 \text{ GHz}/\mu\text{s}$; therefore, the future chirp rate shown below is appropriate. f_m , β , and \mathcal{F} denote the modulation frequency, modulation depth, and finesse, respectively.

	Present	Future	Requirements
Wavelength	243 nm	243 nm	243 nm
Pulse energy	1 mJ	1 mJ	$40 \mu\text{J}$
Time width	500 ns	500 ns	300 ns
Spectral width	17 GHz	150 GHz	140 GHz
Frequency chirp	$\pm 42 \text{ GHz}/\mu\text{s}$	$\pm 378 \text{ GHz}/\mu\text{s}$	$+200 \text{ GHz}/\mu\text{s}$
f_m	78.7 MHz	$78.7 \text{ MHz} \times 3$	
β	2.3 rad	$2.3 \text{ rad} \times 3$	
\mathcal{F}	122	122	

applying these reasonable improvements to the present setup.

The method of optical frequency extension introduced in this paper provides more degrees of freedom for the formation of the frequency chirp. The extension method may be applied to the cooling of various other physical systems by appropriately designing the FSR and gain in the CPTG. For example, by setting a smaller FSR and introducing a gain medium with high controllability in the time domain, it is possible to prepare a spectrally dense, broadband, chirped laser with the desired duration. Such a light source could be applied to chirped cooling of atomic and molecular gases. The controllable gain medium to be introduced into the CPTG could be a semiconductor optical amplifier or a fiber amplifier.

VI. CONCLUSION

We demonstrate the CPTG, a laser system comprising a pulsed laser with an EOM and a pulsed gain medium in the laser cavity. With our prototypical laser, we achieve a 500-ns-long-pulsed, broadband (17 GHz) laser with a chirp rate of ± 42 GHz/ μ s at 243 nm by amplifying the output of the CPTG and generating the third harmonics. Further, as the spectrum of the entire pulse, large spectral broadening spanning over 200 GHz is achieved. We conduct numerical analysis of the CPTG in the time domain, the results of which are in reasonable agreement with our experimental results. In addition, we formulate the temporal and spectral structures of CPTG. A unique feature of the CPTG concept is that it provides more degrees of freedom in chirp formation through the design of the gain medium, resonator, and modulation frequency. This feature can be applied to improve the efficiency of laser cooling in various physical systems.

We also discuss the potential of the third harmonics of the amplified CPTG as a cooling laser for Ps. We show that setting a proper laser cavity FSR for the CPTG, by considering the natural linewidth of the transition and the finite lifetime of Ps, is another essential requirement. The present laser can demonstrate laser cooling of a small amount of the Doppler-broadened Ps gas at room temperature, under realistic experimental conditions. Using the formulas that we develop for the CPTG, we explain how a special laser can be constructed to realize efficient cooling of Ps from 300 to 10 K. We believe that this study could be an essential stepping stone toward high-resolution laser spectroscopy and the creation of quantum degenerate gases of Ps atoms.

ACKNOWLEDGMENTS

This work is supported by JSPS KAKENHI Grants No. JP17H06205, No. JP20K05357, and MEXT Quantum Leap Flagship Program (MEXT Q-LEAP) Grant No. JPMXS0118067246. Y.T. acknowledges the support by

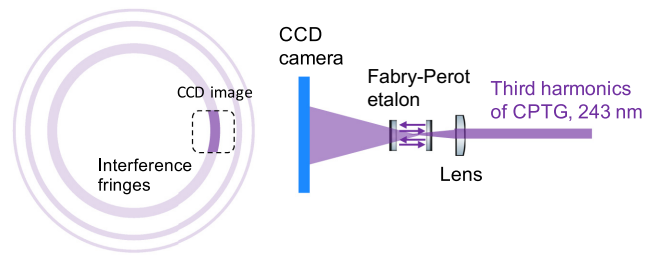


FIG. 11. Schematic of the etalon-based spectrometer. The width of an interference fringe corresponds with the spectral width of the input laser.

FoPM, WINGS Program, The University of Tokyo. E.C. acknowledges the support by National Research Foundation of Korea Grants No. 2020R1A4A1018015 and No. 2020R1F1A1074162. K.Y. acknowledges the support from The University of Tokyo Excellent Young Researcher Program.

APPENDIX: SPECTRAL MEASUREMENT

1. Setup

Figure 11 shows a schematic of the etalon-based spectrometer. We perform shot-by-shot spectrum measurements by sending spatially focused beams to an etalon and by observing the interference fringes using a CCD camera [22].

Figure 12 shows the typical fringe pattern of the third harmonics of the amplified CPTG, obtained using the etalon-based spectrometer. The left panel shows a raw CCD image, while the right panel shows a sliced profile that corresponds to the projection of the shaded region in the left panel on the x axis. As the position in the x axis corresponds to the optical frequency, we can reproduce the optical spectrum by correlating the position with the actual optical frequency. The calibration procedure is described in the following subsection.

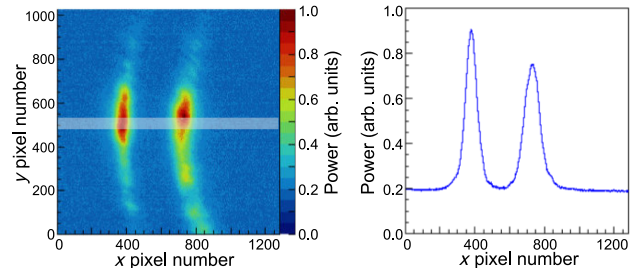


FIG. 12. Typical interference fringe pattern of the third harmonics of the amplified CPTG, measured at 243 nm. The image is averaged over 48 shots. The left panel shows a raw CCD image, wherein the shaded region represents the region of interest for obtaining the right image, which shows a sliced power distribution.

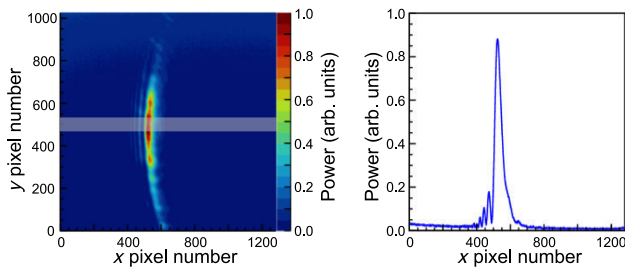


FIG. 13. Typical interference fringe obtained using the etalon-based spectrometer operating at 243 nm, when the input is the third harmonics of the amplified single-mode pulses without EO phase modulation. The image is averaged over 48 shots. The left panel shows a typical raw CCD image, while the right panel shows a sliced power distribution. The small fringe structures seen in the right panel are caused by a nonideal effect of the etalon, which is slightly misaligned [29].

We also build an etalon-based spectrometer operating at 729 nm to observe the output spectrum of the CPTG. However, this spectrometer is unable to resolve the spectrum clearly. The output beam contained the cw laser beam that is reflected from the output coupler mirror in the laser cavity. As we could not reduce the exposure time of the CCD camera to the pulse duration of the output pulse, the signal could not be resolved for the CPTG due to the strong background contribution of the cw laser. Contrarily, only the amplified CPTG pulses survived, after generating the third harmonics, because of the nonlinear optical processes. Consequently, we use the spectrometer only at 243 nm to evaluate the spectrum of the pulsed light.

2. Calibration of the spectrometer

The calibration process of the spectrometer is as follows. Figure 13 shows the typical fringe patterns of the third harmonics of the amplified CPTG without EO modulation, obtained using the etalon-based spectrometer. The left panel shows a raw CCD image, while the right panel shows

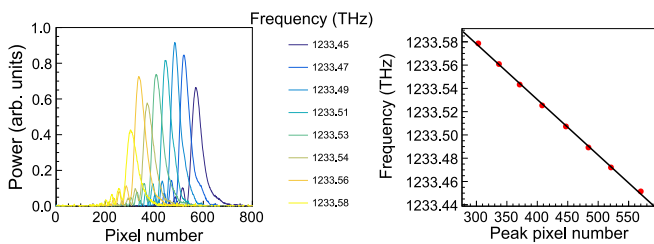


FIG. 14. The left panel shows the instrumental function of the etalon-based spectrometer when the optical frequency of the input single-mode pulsed laser is varied. The right panel shows the correspondence between the optical frequency and the position on the CCD. The red dot denotes the peak pixel number of the corresponding curve in the left panel, and the solid line represents the fitting result with a linear polynomial function.

a sliced profile. Since the input is single-longitudinal-mode pulsed light at 243 nm, and linewidth is much narrower than the resolution of the etalon. Therefore, the right panel of Fig. 13 shows the instrumental function of the spectrometer at 243 nm.

The left panel of Fig. 14 shows the instrumental function of the spectrometer when the optical frequency of the single-mode pulsed laser is varied. Meanwhile, we measure the optical frequency of the single-mode pulse by tripling the measured optical frequency of the seed laser at 729 nm using a wavelength meter (WS7-60, HighFinesse GmbH). The right panel shows the correspondence between the optical frequency and the peak pixel number. The data are fitted using a linear polynomial function, and the fitting result is used to convert the arbitrary pixel number of the CCD into the optical frequency.

- [1] M. S. Fee, A. P. Mills Jr., S. Chu, E. D. Shaw, K. Danzmann, R. J. Chichester, and D. M. Zuckerman, Measurement of the Positronium $1_1^{3S} - 2_1^{3S}$ Interval by Continuous-Wave Two-Photon Excitation, *Phys. Rev. Lett.* **70**, 1397 (1993).
- [2] M. S. Fee, S. Chu, A. P. Mills Jr., R. J. Chichester, D. M. Zuckerman, E. D. Shaw, and K. Danzmann, Measurement of the positronium $1_1^{3S} - 2_1^{3S}$ interval by continuous-wave two-photon excitation, *Phys. Rev. A* **48**, 192 (1993).
- [3] S. G. Karshenboim, Precision study of positronium: Testing bound state QED theory, *Int. J. Mod. Phys. A* **19**, 3879 (2004).
- [4] G. S. Adkins, M. Kim, C. Parsons, and R. N. Fell, Three-Photon-Annihilation Contributions to Positronium Energies at Order $m\alpha^7$, *Phys. Rev. Lett.* **115**, 233401 (2015).
- [5] D. B. Cassidy and A. P. Mills Jr., Physics with dense positronium, *Phys. Stat. Solidi (c)* **4**, 3419 (2007).
- [6] V. Vanyashin, Coherent decay of positronium bose condensate, *Lett. Math. Phys.* **31**, 143 (1994).
- [7] A. P. Mills Jr., D. B. Cassidy, and R. Greaves, Prospects for making a bose–einstein-Condensed positronium annihilation gamma ray laser, *Mater. Sci. Forum* **445-446**, 424 (2004).
- [8] H. K. Avetissian, A. K. Avetissian, and G. F. Mkrtchian, Self-Amplified Gamma-Ray Laser on Positronium Atoms from a Bose-Einstein Condensate, *Phys. Rev. Lett.* **113**, 023904 (2014).
- [9] S. Mariuzzi, P. Bettotti, and R. S. Brusa, Positronium Cooling and Emission in Vacuum from Nanochannels at Cryogenic Temperature, *Phys. Rev. Lett.* **104**, 243401 (2010).
- [10] A. P. Mills Jr., Positronium bose–einstein condensation in liquid ^4He bubbles, *Phys. Rev. A* **100**, 063615 (2019).
- [11] D. B. Cassidy, Experimental progress in positronium laser physics, *Eur. Phys. J. D* **72**, 53 (2018).
- [12] K. Shu, X. Fan, T. Yamazaki, T. Namba, S. Asai, K. Yoshioka, and M. Kuwata-Gonokami, Study on cooling of positronium for bose–einstein condensation, *J. Phys. B: At., Mol. Opt. Phys.* **49**, 104001 (2016).

- [13] E. P. Liang and C. D. Dermer, Laser cooling of positronium, *Opt. Commun.* **65**, 419 (1988).
- [14] H. Iijima, T. Hirose, M. Irako, M. Kajita, T. Kumita, H. Yabu, and K. Wada, Monte carlo study of ortho-positronium laser cooling, *J. Phys. Soc. Jpn.* **70**, 3255 (2001).
- [15] T. Kumita, T. Hirose, M. Irako, K. Kadoya, B. Matsumoto, K. Wada, N. N. Mondal, H. Yabu, K. Kobayashi, and M. Kajita, Study on laser cooling of ortho-positronium, *Nucl. Instrum. Methods Phys. Res. B* **192**, 171 (2002).
- [16] W. D. Phillips, Nobel lecture: Laser cooling and trapping of neutral atoms, *Rev. Mod. Phys.* **70**, 721 (1998).
- [17] Y. Kataoka, S. Asai, and T. Kobayashi, First test of $O(\alpha^2)$ correction of the orthopositronium decay rate, *Phys. Lett. B* **671**, 219 (2009).
- [18] M. Kourogi, K. Nakagawa, and M. Ohtsu, Wide-span optical frequency comb generator for accurate optical frequency difference measurement, *IEEE J. Quantum Electron.* **29**, 2693 (1993).
- [19] K.-P. Ho and J. M. Kahn, Optical frequency comb generator using phase modulation in amplified circulating loop, *IEEE Photon. Technol. Lett.* **5**, 721 (1993).
- [20] T. W. Hänsch and B. Couillaud, Laser frequency stabilization by polarization spectroscopy of a reflecting reference cavity, *Opt. Commun.* **35**, 441 (1980).
- [21] W. H. Lowdermilk and J. E. Murray, The multipass amplifier: Theory and numerical analysis, *J. Appl. Phys.* **51**, 2436 (1980).
- [22] A. Deller, B. S. Cooper, T. E. Wall, and D. B. Cassidy, Positronium emission from mesoporous silica studied by laser-enhanced time-of-flight spectroscopy, *New J. Phys.* **17**, 043059 (2015).
- [23] A. Yariv and P. Yeh, *Photonics: Optical Electronics in Modern Communications* (Oxford University Press, New York, 2007).
- [24] G. M. Macfarlane, A. S. Bell, E. Riis, and A. I. Ferguson, Optical comb generator as an efficient short-pulse source, *Opt. Lett.* **21**, 534 (1996).
- [25] S. Xiao, L. Hollberg, N. R. Newbury, and S. A. Diddams, Toward a low-jitter 10 GHz pulsed source with an optical frequency comb generator, *Opt. Exp.* **16**, 8498 (2008).
- [26] L. M. Frantz and J. S. Nodvik, Theory of pulse propagation in a laser amplifier, *J. Appl. Phys.* **34**, 2346 (1963).
- [27] D. B. Cassidy, P. Crivelli, T. H. Hisakado, L. Liskay, V. E. Meligne, P. Perez, H. W. K. Tom, and A. P. Mills Jr., Positronium cooling in porous silica measured via doppler spectroscopy, *Phys. Rev. A* **81**, 012715 (2010).
- [28] P. Del’Haye, S. B. Papp, and S. A. Diddams, Hybrid Electro-Optically Modulated Microcombs, *Phys. Rev. Lett.* **109**, 263901 (2012).
- [29] G. Xia, Z. Wu, M. Liu, and Y. Pan, Transmitted characteristics for a Gaussian beam passing through a misaligned fabry-perot interferometer, *Optik* **114**, 521 (2003).